ACS Sustainable Chemistry & Engineering

Research Article

Cite This: ACS Sustainable Chem. Eng. 2018, 6, 4948−4957

pubs.acs.org/journal/ascecg

Silver Nanoparticle-Decorated Boron Nitride with Tunable Electronic Properties for Enhancement of Adsorption Performance

Jingyu Pang,[†,‡] Yanhong Chao,[*,§] Honghong Chang,[‡] Hongping Li,[‡] Jun Xiong,[‡] Qi Zhang,[‡] Guangying Chen,[∥] Junchao Qian,[⊥] Wenshuai Zhu,[*,‡] and Huaming Li[‡]

[†]School of Food and Biological Engineering, Jiangsu University, 301 Xuefu Road, Zhenjiang, Jiangsu 212013, P. R. China

[‡]School of Chemistry and Chemical Engineering, Jiangsu University, 301 Xuefu Road, Zhenjiang, Jiangsu 212013, P. R. China

[§]School of Pharmacy, Jiangsu University, 301 Xuefu Road, Zhenjiang, Jiangsu 212013, P. R. China

[∥]Key Laboratory of Tropical Medicinal Plant Chemistry of Ministry of Education, Hainan Normal University, 99 South Longkun Road, Haikou, Hainan 571158, P. R. China

[⊥]Jiangsu Key Laboratory of Environment Functional Materials, Suzhou University of Science and Technology, 1 Kerui Road, Suzhou, Jiangsu 215009, P. R. China

Supporting Information

ABSTRACT: In this paper, a series of silver nanoparticle (AgNP)-decorated boron nitride (Ag-BN) with different Ag amounts were successfully synthesized by a one-pot pyrolysis method and used as novel high-efficiency adsorbents for the removal of organic pollutant tetracycline (TC) and rhodamine B (RhB). According to the adsorption capacity of the samples, the obtained optimal Ag/B molar ratio was 1%. The adsorption data fitted well with the pseudo-second-order kinetics and Langmuir isotherm models with the maximum adsorption capacity of 358 and 880 mg/g for TC and RhB, respectively. The thermodynamic studies suggested that the adsorption process was spontaneous and endothermic in nature. The introduction of AgNP onto BN enhanced the adsorption capacity on account of tunable electronic properties. The adsorption mechanism is discussed in detail with the effect of pH, density function theory (DFT), and thermodynamics.

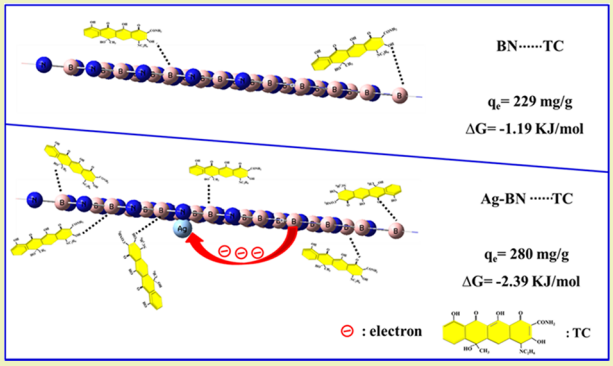

KEYWORDS: *Boron nitride, Organic pollutant removal, Adsorption mechanism*

INTRODUCTION

With ever-increasing attention to the water environment, there is now a great deal of demand for the removal of organic pollutants from wastewater. The organic pollutants containing benzene rings are generally residual in the environment and harmful to public health. Different technologies for treating water pollutants have been proposed, such as coagulation,[1−3] adsorption,[4−7] hydrolysis,[8,9] photocatalysis,[10−12] and electrochemistry,[13−15] as well as biodegradation.[16−18] Among which, adsorption is selected as a much potential process because of the low cost, easy operation, outstanding designability, and high efficiency.[19−22]

Up to now, different nanomaterials have been control-prepared as adsorbents in order to acquire desired adsorption performance, such as FeOOH,[23,24] MnO_2,[25,26] WO_3,[27,28] MOF,[29,30] thermoresponsive polymers[31−33] and so on. Each of the materials has inherent limitations, and their structures are unstable in an harsh environment.[34] Boron nitride (BN), as an analogue of graphite, has aroused much attention due to its being lightweight and having large specific areas, thermal stability, and chemical inertness.[35−39] In recent years, BN was investigated and employed widely for adsorption. Lei et al. reported that porous BN nanosheets had a superior adsorption for oils, solvents, and dyes.[19] Zhang et al. fabricated the mesoporous hexagonal boron nitride fibers, which had high adsorption capacity for organic pollutants.[40] Yu et al. synthesized nanosheet-structured boron nitride spheres and applied for water cleaning.[41] Tang et al. prepared porous hexagonal BN and studied the adsorption performance for tetracyclines.[42] Furthermore, several modification methods were also used to enhance the adsorptive capacity of BN. Mechanical solid-state exfoliation was used to modify BN (7 h for mill and 1 h for pyrolysis) and exhibited high lysozyme adsorption performance and excellent recyclability.[43] Acid solution was introduced to activate BN fibers (8.5 h for synthesis and treatment) in order to expose more active sites and enhance the adsorption behavior.[44] These modifications of BN can efficiently improve the adsorption performance.

Received: November 28, 2017
Revised: January 30, 2018
Published: February 26, 2018

DOI: 10.1021/acssuschemeng.7b04481
ACS Sustainable Chem. Eng. 2018, 6, 4948−4957

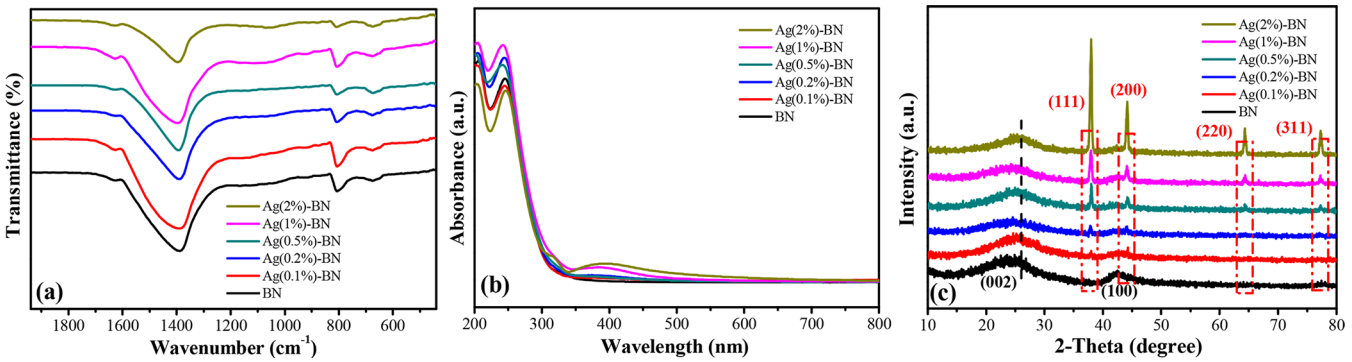

Figure 1. FTIR spectra (a), UV−vis DRS (b), and XRD pattern (c) of Ag-BN with different Ag amounts.

However, the processes are time consuming and complex operations. Therefore, the development of new modifications with simple operations is highly desirable.

In our previous work, we found that the electronic properties of BN played a significant role in adsorption,[34,45] and the Lewis acid−base interaction was also demonstrated according to the density function theory (DFT).[46,47] Both experimental and theoretical studies confirmed that the adsorptive activity of BN was related to its electronic properties. Recently, silver nanoparticle (AgNP) has been proposed as modified materials in many fields, such as surface-enhanced Raman spectroscopy,[48,49] reduction reaction,[50,51] and lithium ion batteries[52,53] due to the excellent electrical conductivity and charge mobility. Therefore, the superiority of BN and AgNP motivated us as to whether we could design an appropriate and simple strategy to couple them for more efficient adsorption.

In this study, we demonstrate a one-pot pyrolysis strategy for the in situ synthesis of AgNP-decorated boron nitride (Ag-BN) with tunable AgNP loading amounts for enhancing the adsorption behavior of tetracycline (TC) and rhodamine B (RhB). The adsorption activity, including adsorption kinetics, isotherms, thermodynamics, pH effect, and recycling are investigated systematically. Additionally, the adsorption mechanism is discussed further.

EXPERIMENTAL SECTION

Materials. Boric acid (GR, ≥ 99.8%), urea (AR, ≥ 99.0%), silver nitrate ($AgNO_3$, AR, ≥ 99.8%), and methanol (GR, ≥ 99.7%) were purchased from Sinopharm Chemical Reagent. Tetracycline (TC, > 98.0%) and rhdamine B (RhB, 95.0%) were purchased from Sigma-Aldrich.

Synthesis. In a typical synthetic method, boron acid, urea, and $AgNO_3$ were dissolved in a methanol aqueous solution[54] with a molar ratio of 1:30:X. The mixture was heated at 55 °C until the solution was boiled away. The obtained light gray powders were calcined at 900 °C for 5 h in a N_2 atmosphere. The obtained products were designed as Ag(X)-BN, where X was 0.1%, 0.2%, 0.5%, 1%, and 2%. For comparison, pure BN was also prepared by the same procedure without adding $AgNO_3$.

Characterization. FT-IR spectra were recorded on a Nexus 470 spectrometer from 4000 to 400 cm^{-1} using powder-pressed KBr pellets at room temperature. Ultraviolet−visible diffuse reflectance spectra (UV−vis DRS) in this system were obtained via a UV−vis spectrometer (Shimadzu UV-2450 spectrophotometer) by a diffuse reflectance method with $BaSO_4$ powder as the substrate. The phase structural characteristics of the samples were determined by X-ray diffractometry (XRD) using a Bruker D8 diffractometer with Cu Kα radiation. The chemical states of the prepared samples were analyzed by X-ray photoelectron spectroscopy (XPS) using a VG MultiLab 2000 spectrometer using Mg KR (1253.6 eV) radiation. The morphology of the sample was investigated by a scanning electron microscope (SEM) (JEOL JSM-7001F). The pH values of the reaction solutions were measured using a pH meter (Starter 2100, Ohaus Instruments Co., Ltd.). The nitrogen adsorption−desorption isotherms were obtained using a TriStar II 3020 surface area and porosity analyzer (Micromeritics Instrument Corporation, USA).

Adsorption. Batch adsorption experiments were carried out at room temperature to investigate the adsorption behaviors of TC/RhB onto Ag-BN with different Ag amounts. Typically, the sample (5.0 mg) was placed into 25 mL aqueous solutions containing one of the pollutants with different concentrations in a flask and shaken in a rotary shaker for a period of time to reach adsorption equilibrium. The concentration of pollutants was determined by a UV−vis spectrophotometer (UV-2501) based on the standard curve. The equilibrium adsorption capacity (q_e) was calculated on the basis of the eq 1.

$$q_e = \frac{(C_0 - C_e)V}{m} \quad (1)$$

where C_0 and C_e are the initial and the equilibrium concentrations of pollutants in the test solution (mg/L), V is the volume of the testing solution (L), and m is the weight of the adsorbent (g).

The initial pH of the TC solution was adjusted in the range of 2−10 using NaOH or HCl solutions to study the effect of initial solution pH on TC adsorption by Ag(1%)-BN. Adsorption isotherms were conducted with initial concentrations ranging from 100 to 300 mg/L. For regeneration, the TC-adsorbed Ag(1%)-BN was washed with ethanol for 2 h to reach desorption equilibrium. Then, the mixed solids were washed several times with ethanol and reused in adsorption experiments. The process was repeated five times.

RESULTS AND DISCUSSION

Characterization of Samples. FTIR spectra of Ag-BN with different Ag amounts are shown in Figure 1a. Two characteristic peaks around 1380 and 800 cm^{-1} were attributed to the vibrations of B−N stretching and B−N bending, respectively.[41] The FTIR spectra of Ag-BN were very similar to that of pristine BN. The results revealed that the original *h*-BN framework remained almost unchanged. Additionally, UV−vis DRS spectra were also used to investigate the chemical component information on samples. The results are shown in Figure 1b. Sharp peaks at 241 nm were found in the spectra of both BN and Ag-BN, which contributed to *h*-BN.[55] It was noted that new peaks around 380 nm emerged distinctly in Ag(1%)-BN and Ag(2%)-BN, which were assigned to the surface plasmon band of silver.[56]

Figure 1c showed the crystallographic structure of the prepared samples in the 2θ range of 10°−80°. Two broad peaks centered at 2θ = 25.68−26.34° and 2θ = 42.48° were indexed to the (002) and (100) crystal planes of BN (JCPDS no. 34-0421).[57] Four distinct diffraction peaks at 2θ = 38.02°, 44.24°,

DOI: 10.1021/acssuschemeng.7b04481
ACS Sustainable Chem. Eng. 2018, 6, 4948−4957

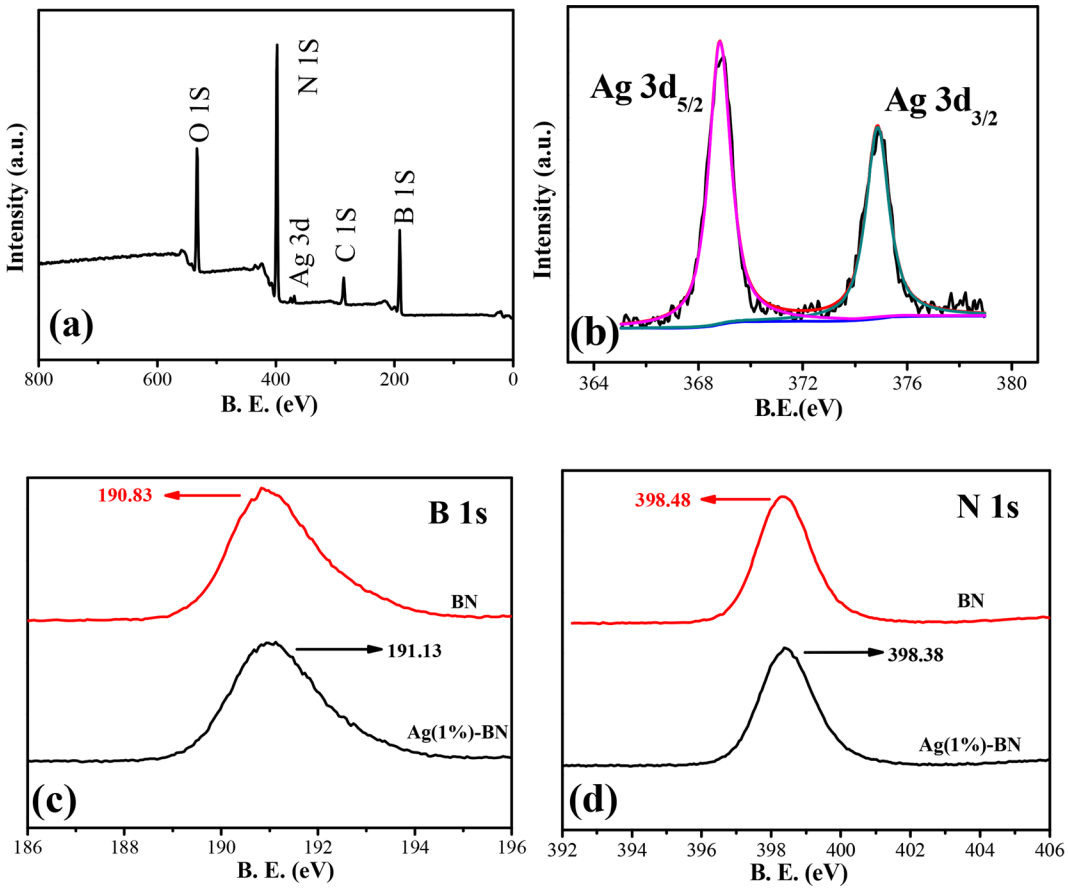

Figure 2. XPS spectra of Ag(1%)-BN: (a) full scan of Ag(1%)-BN, (b) Ag 3d of Ag(1%)-BN, (c) B 1s of BN and Ag(1%)-BN, and (d) N 1s of BN and Ag(1%)-BN.

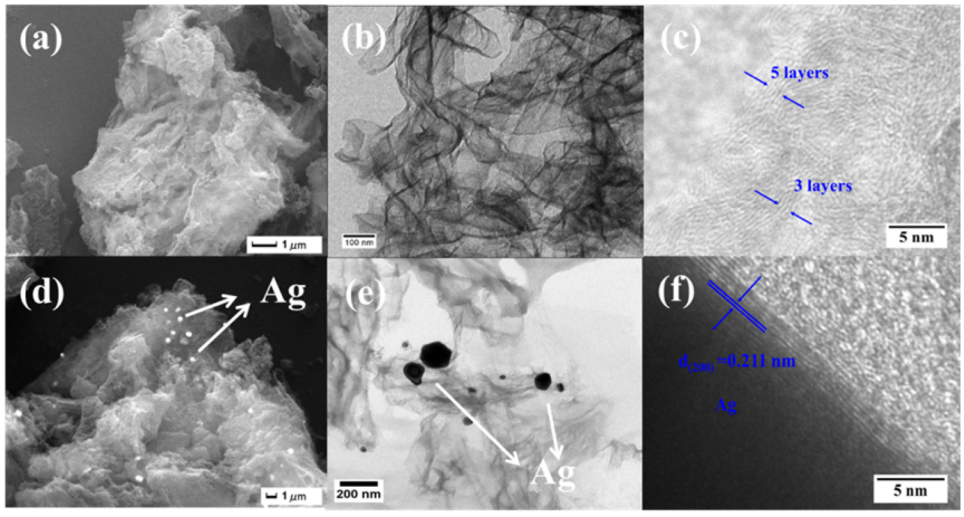

Figure 3. SEM images of BN (a) and Ag(1%)-BN (d). TEM images of BN (b) and Ag(1%)-BN (e). HRTEM images of BN (c) and Ag(1%)-BN (f).

64.32° and 77.3° corresponding to the (111), (200), (220) and (311) planes of Ag(0) (JCPDS no. 04-0783) were observed for Ag-BN samples.[58] The intensity of the characteristic peak intensified gradually with the increase in the AgNP concentration. In addition, the (002) diffraction peak shifted slightly to higher angles along with the increase in the AgNP concentration. According to the Bragg eq ($2d \times \sin\theta = n\lambda$), the (002) diffraction peak shifted slightly to a higher angle, indicating the decrease in the interplanar distance.[34] *h*-BN typically exhibited AA′ stacking, in which each B atom eclipses with an N atom on the adjacent layer due to favorable electrostatic interaction.[36,59] In the following XPS part, it had been proved that the B atom tended to be more positively charged. Then, the interaction of interlayer stacking may become stronger due to the increasing of electrostatic interaction, resulting in the decrease in the interplanar distance. Most probably, the shift in the (002) peak was attributed to the change of electronic properties of the B atom.

DOI: 10.1021/acssuschemeng.7b04481
ACS Sustainable Chem. Eng. 2018, 6, 4948−4957

X-ray photoelectron spectroscopies (XPS) were investigated to ascertain chemical states and electron transfer of BN and Ag(1%)-BN. As depicted in Figure 2a, B, N, O, C, and Ag are detected in Ag(1%)-BN. In the high-resolusion XPS spectra of Ag in Ag(1%)-BN (Figure 2b), two peaks at binding energies of 368.8 and 374.9 eV are observed and ascribed to the Ag $3d_{5/2}$ and Ag $3d_{3/2}$, respectively, which indicated that silver was present only in metallic form.[60,61] This can be taken as additional evidence for the formation of Ag(0). To further discuss the effect of AgNP, the high-resolusion XPS spectra of B and N in BN and Ag(1%)-BN were also investigated, respectively. As shown in Figure 2c, the bonding energy for B 1S in Ag(1%)-BN has shifted to a higher value compared to BN. This shift demonstrated that some electrons deviated away from the B atom, implying that the B atom tended to be more electropositive.[62] In Figure 2d, the slight variation of N 1S is also observed due to the decorating of AgNP. Therefore, boron can present increased electropositivity when decorated with AgNP.

The SEM image in Figure 3a shows BN with a fluffy cloud-like sheet structure. Figure 3d is the SEM image of Ag(1%)-BN, which shows that Ag(1%)-BN also had the fluffy structure, and AgNP on the surface of BN can be seen clearly. Additionally, the typical TEM images of BN and Ag(1%)-BN (Figure 3b, e) illustrated the curled sheets microscopic structure of BN, and the AgNP was anchored onto the BN nanosheets. The size distribution of AgNP is shown in Figure S1, and the average size was 176 nm. Figure 3c shows the HRTEM image of BN. The disordered lattice fringes could be observed due to the poor crystallinity, which is supported by XRD. The formation of Ag(1%)-BN was further confirmed by HRTEM (Figure 3f). It can be seen that AgNP had distinct lattice spacing of 0.211 nm, corresponding to the (200) crystal plane of Ag(0) (JCPDS no. 04-0783). The above results indicated that AgNP had been decorated on BN successfully.

The N_2 adsorption−desorption isotherms of adsorbents are illustrated in Figure S2. It can be seen that all isotherms conformed to type II based on the IUPAC classification, and the type H3 hysteresis indicated the presence of slits pores stacked by the layer structure. The pore size distributions obtained by the DFT model presented the probable pore size centered about 2 nm, which also indicated the microporosity of BN. Table 1 displays the textural properties of BN samples,

Table 1. Texture Properties of Ag-BN with Different Ag Amounts

Sample	S_{BET} (m^2/g)	Pore size (nm)
BN	1101	2.1
Ag(0.1%)-BN	1161	2.3
Ag(0.2%)-BN	1148	2.1
Ag(0.5%)-BN	1357	2.1
Ag(1%)-BN	1378	2.1
Ag(2%)-BN	834	2.4

which is calculated by the Brunauer−Emmett−Teller (BET) specific surface area (S_{BET}). The Ag(1%)-BN possessed the largest S_{BET} of 1378 m^2/g. But when the content of Ag increased to 2%, the value of S_{BET} decreased to 834 m^2/g. This may be due to the structural pore collapse or the excess aggregation of Ag nanoparticles.

Effect of Content of AgNP on Adsorption. The adsorption capacities of Ag-BN with different Ag amounts for TC/RhB were explored with an initial concentration of 200 mg/L and a temperature of 298 K. The measured adsorption capacities of all the samples are shown in Figure 4. Based on the experimental results, it can be found that suitable decorated content of 1% AgNP on BN exhibited the best adsorption capacity.

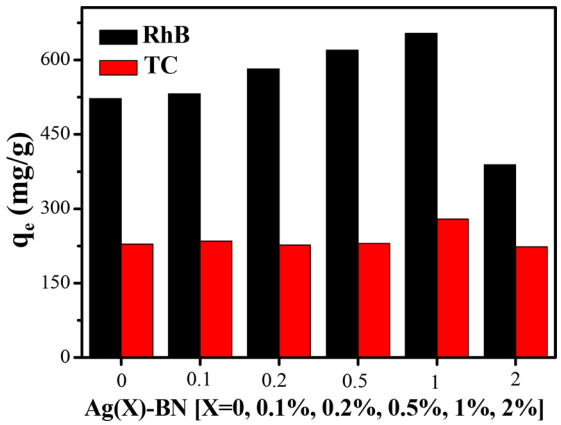

Figure 4. Adsorption capacity of TC/RhB for Ag-BN with different Ag amounts.

We proposed that the enhancement of adsorption capacities was due to the interfacial coupling between Ag and BN with the introduction of appropriate content AgNP onto BN. The decoration of AgNP on BN would reduce the outer surface electron cloud density of BN and increase the electropositivity of B atoms, which were demonstrated in the XPS part. As we all know, Lewis acid−base interaction plays a significant role in adsorptive behavior. In this system, BN acted as a Lewis base due to the virtual orbitals of the B atoms, and TC/RhB acted as a Lewis acid because of the lone pair electrons in the oxygen atoms. The increased electropositivity of virtual orbitals in the B atoms could build powerful interactions between BN and TC/RhB and result in an enhancement of adsorption capacity. A similar phenomenon was also reported in our previous work.[45] The decrease in adsorption capacity for Ag(2%)-BN may be caused by the aggregation of Ag nanoparticles and the sharply declined specific surface area (Table 1).

Effect of Solution pH on Adsorption. The effect of initial solution pH on TC adsorption onto Ag(1%)-BN was studied within the pH range between 2 and 12 at 298 K with the initial concentration of 200 mg/L. As shown in Figure 5a, the adsorption capacity is observed to decrease with the increase in pH value. It suggested that an acidic condition facilitated TC adsorption. BN has an overall negative surface charge,[63] and TC has three pK_a values, resulting in different charges under different conditions. When the solution pH is below 3.3, TC exists as a cation (TCH_3^+). At pH between 3.3 and 7.7, TC exists as a zwitterion (TCH_2^0). When pH is higher than 7.7, the dominant species become TCH^- and TC^{2-}, which exist as anions.[64,65] At lower pH, the dominant interaction of electrostatic attraction caused a more positively charged TC to absorb onto Ag(1%)-BN. But as pH values increased, the level of deprotonation of TC increased and TCH^- and TC^{2-} became the dominant species gradually. The increase in the proportion of negatively charged TC species resulted in an electrostatic repulsion interaction between TC and negativly charged Ag(1%)-BN, so less TC was adsorbed onto Ag(1%)-BN at higher pH conditions. Therefore, pH played a significant

DOI: 10.1021/acssuschemeng.7b04481
ACS Sustainable Chem. Eng. 2018, 6, 4948−4957

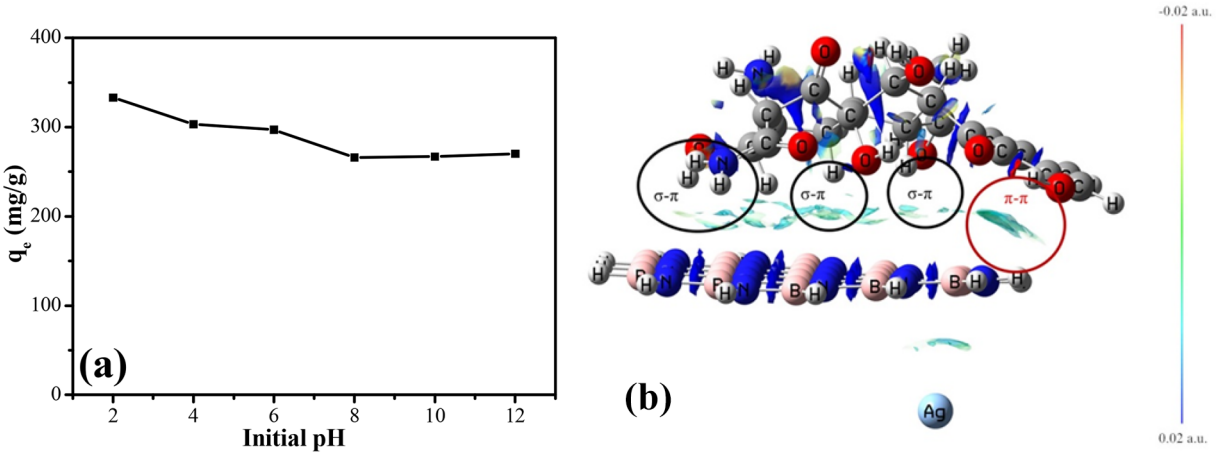

Figure 5. (a) Effect of initial pH on the adsorption of TC onto the Ag(1%)-BN. (b) Gradient isosurfaces (s = 0.35 au) for complex TC-Ag-BN. The surfaces are colored on a red−green−blue scale, ranging from −0.04 to 0.02 au. Red indicates strong attractive interactions. Green indicates typical van der Waals interactions, and blue indicates strong nonbonded overlap.

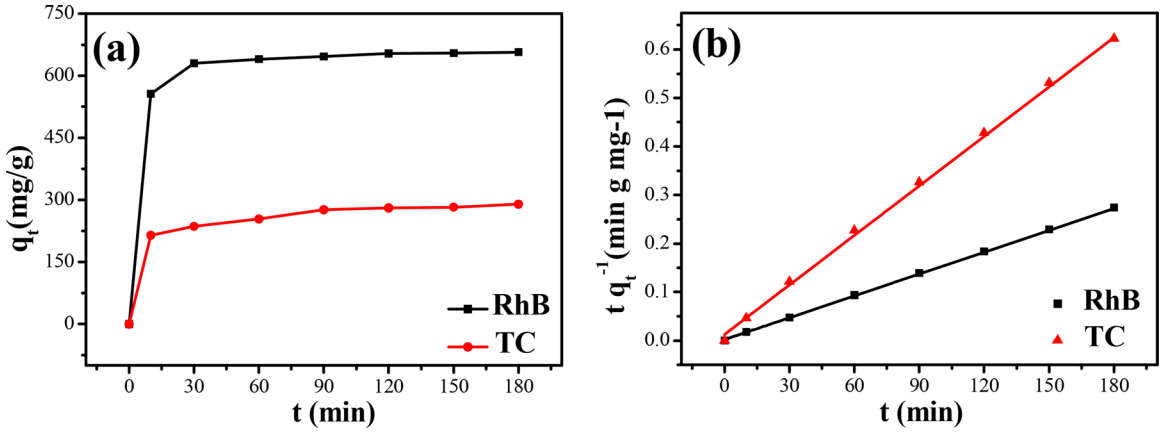

Figure 6. (a) Effects of contact time on the adsorption capacity. (b) Plots of the pseudo-second-order kinetic model of TC/RhB onto Ag(1%)-BN, respectively.

role during the adsorption process due to electrostatic interactions. It is noteworthy that when the pH was greater than 3.3, no electrostatic attraction existed between TC and Ag(1%)-BN. But the adsorption capacity still stayed at a high level. It may profit from the nonelectrostatic $\pi-\pi$ interaction between bulk π systems on the Ag(1%)-BN surface and TC molecules which contained both benzene rings and C═O and C═C.[66]

To better understand the interaction between the TC and Ag(1%)-BN, a density functional theory (DFT, B3LYP/6-31+G(d,p)) calculation was performed. The selected model consisted of a single Ag atom and a cluster of *h*-BN. This computational model was first optimized to a local minimum. Then, the local minimum was analyzed by a reduced density gradient (RDG) algorithm (Figure 5b).[67] The RDG algorithm was a powerful visualized method to understanding the weak interaction.[68] As can be seen from Figure 5b, the colorful areas between TC and Ag(1%)-BN represent the weak interaction between them. It clearly shows that the TC molecule interacted with the substitute by different interaction types. The left three cycles show typical O−H···π, N−H···π, and C−H···π interactions, which can be called $\sigma-\pi$ interactions. The right red cycle shows an interaction between the benzene ring and the *h*-BN surface, which can be called a $\pi-\pi$ interaction. In order to further discuss the interactions, we further extended our analysis to the larger cluster (Ag4 cluster). The RDG surface of the Ag4 cluster model (Figrue S3) got the same results with a single Ag model, which was conformed to the interaction nature in the current system. Hence, it can be concluded that $\sigma-\pi$ and $\pi-\pi$ interactions between TC and Ag(1%)-BN also played an important part during the adsorption process. Combined with the above analysis, the adsorption mechanism was $\sigma-\pi$ and $\pi-\pi$, and the electrostatic interactions which deduced from the results of pH effect.

Adsorption Kinetics. Equilibrium time and kinetics parameters are some of the most significant parameters during the adsorption process. The effect of contact time for TC/RhB adsorption onto Ag(1%)-BN at 298 K is shown in Figure 6a. The adsorption capacity was increased rapidly and gradually tended to be steady up to 120 min. Further increase in the contact time did not cause any obvious rise due to the equilibrium of surface sites for adsorption.[69] Therefore, the adsorption equilibration time was selected at 120 min. Two kinetic models, pseudo-first-order and pseudo-second-order, were used to investigate the adsorption behavior which is shown in eqs 2 and 3, respectively.

$$lg(q_e - q_t) = lg\, q_e - k_1 t \quad (2)$$

DOI: 10.1021/acssuschemeng.7b04481
ACS Sustainable Chem. Eng. 2018, 6, 4948−4957

Table 2. Kinetic Parameters for TC/RhB Adsorption onto Ag(1%)-BN at 298 K

	Pseudo-first order			Pseudo-second order			
	q_e (mg/g)	k_1 (min^{-1})	R^2	q_e (mg/g)	$t_{1/2}$ (min)	k_2 ($g{\cdot}mg^{-1}{\cdot}min^{-1}$)	R^2
TC	154	0.026	0.831	294	3.74	0.0009	0.999
RhB	235	0.033	0.722	667	1.33	0.0011	0.999

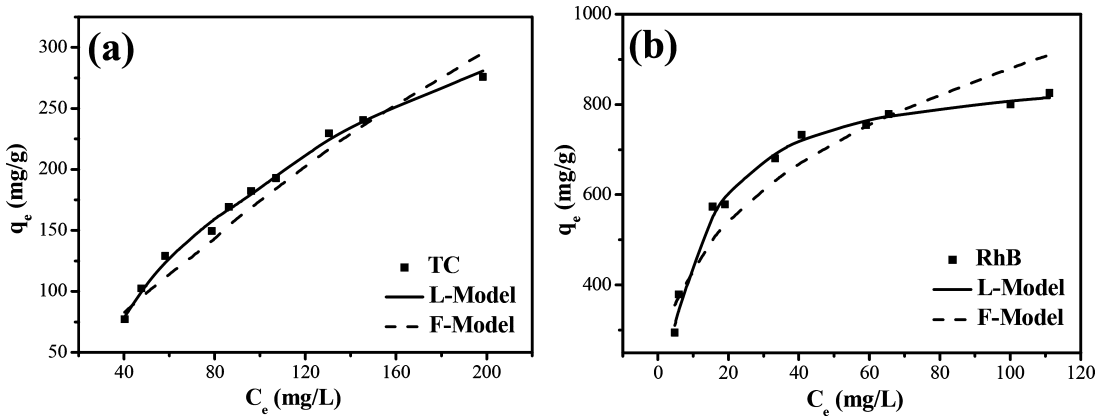

Figure 7. Langmuir and Freundlich isotherms of TC (a) and RhB (b) adsorption on Ag(1%)-BN.

Table 3. Isotherm Parameters of TC and RhB Adsorption on Ag(1%)-BN at 298 K

	Langmuir				Freundlich			
	q_m (mg/g)	K_L (L/mg)	R^2	*APE*%	K_F (L/mg)	n	R^2	*APE*%
TC	358	0.009	0.990	2.7	12.50	1.71	0.965	7.7
RhB	880	0.113	0.984	2.0	221	3.33	0.918	4.8

$$\frac{t}{q_t} = \frac{1}{k_2 q_e^2} + \frac{t}{q_e} \tag{3}$$

where q_e and q_t (mg/g) are the adsorption capacity at equilibrium time and time t, respectively. k_1 (min^{-1}) and k_2 ($g{\cdot}mg^{-1}{\cdot}min^{-1}$) are the rate constant of pseudo-first-order model and pseudo-second-order models, respectively. The corresponding parameters calculated from the above two equations are listed in Table 2. The plots of the pseudo-second-order kinetic model are shown in Figure 6b. According to the correlation coefficient R^2, the adsorption behavior can be described well with the pseudo-second-order model.[70] $t_{1/2}$ reflects the time when q_t reached one-half of q_e ($t_{1/2} = k_2^{-1} q_e^{-1}$). $t_{1/2}$ with a short time (3.74 and 1.33 min) indicated that the adsorption behavior of TC/RhB onto Ag(1%)-BN had a rapid adsorption rate.

Adsorption Isotherms. The adsorption isotherm, providing the surface properties of adsorbents, is necessary to establish the distribution of adsorbates between the liquid phase and the solid phase. Langmuir and Freundlich models are the most common models to evaluate the adsorption equilibrium.

The Langmuir isotherm

$$\frac{C_e}{q_e} = \frac{C_e}{q_m} + \frac{1}{q_m K_L} \tag{4}$$

where C_e (mg/L) is the equilibrium concentration of TC/RhB, q_e (mg/L) is the adsorption capacity at the equilibrium point, q_m (mg/g) is the maximum adsorption capacity, and K_L is the Langmuir constant.

The Freundlich isotherm

$$q_e = K_F C_e^{1/n} \tag{5}$$

where C_e and q_e are the same as defined above, K_F is the Frendlich constant, and n is the adsorption intensity.

The average percentage error (*APE*%) is written as

$$APE\% = \sum_{i=1}^{N} |(q_{e,exp} - q_{e,cal})/q_{e,exp}|/N \times 100 \tag{6}$$

where $q_{e,exp}$ and $q_{e,cal}$ are the adsorption capacity of experimental value and calculated value by the isotherm models, respectively. N is the number of experiment data points. The Langmuir and Freundlich isotherms are shown in Figure 7. q_m, K_L, n, K_F, and *APE*% can be calculated by eqs 4−6, and the results are shown in Table 3. For the adsorption of TC/RhB, higher correlation coefficient R^2 and lower *APE*% values of Langmuir fitting suggested that Langmuir was the better isotherm model for describing the adsorption process onto Ag(1%)-BN than the Freundlich model, and the adsorption was proposed as monolayer adsorption on the surface of Ag(1%)-BN. The obtained maximum adsorption capacity (q_m) of TC and RhB was 358 and 880 mg/g, respectively. Compared with some reported adsorbents (listed in Table S1), Ag-BN was a good candidate for adsorption.

Adsorption Thermodynamics. Thermodynamics estimated in different temperatures (298−328 K) would reflect the thermodynamic feasibility and spontaneous nature of the adsorption process, and the parameters are calculated according to the follow equation[71]

$$\ln K = \frac{\Delta S}{R'} - \frac{\Delta H}{R'T} \tag{7}$$

DOI: 10.1021/acssuschemeng.7b04481
ACS Sustainable Chem. Eng. 2018, 6, 4948−4957

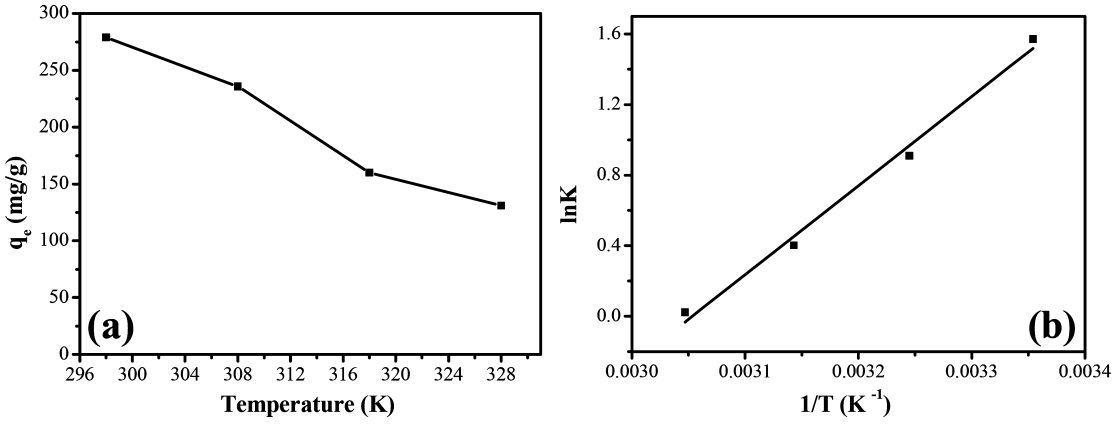

Figure 8. (a) Effect of temperature on adsorption of TC onto Ag(1%)-BN (a). (b) Regressions of van't Hoff for thermodynamic parameters.

Table 4. Thermodynamic Parameters for Adsorption of TC onto BN and Ag(1%)-BN

	ΔG (kJ/mol)					
Adsorbents	289 K	308 K	318 K	328 K	ΔH (kJ/mol)	ΔS (J/(mol·K))
BN	−1.19	−0.76	−0.36	−0.0084	−12.93	−39.47
Ag(1%)-BN	−2.39	−1.71	−0.70	−0.040	−26.42	−80.54

$$\Delta G = -R'T\ln K \quad (8)$$

where R' (8.314 J/(mol·K)) is the gas constant, T (K) is the system temperature, and K is thermodynamic equilibrium constant ($K = \ln q_e/C_e$). As shown in Figure 8a, the adsorption capacity appears as a decreasing trend with the rise in temperature. The results suggested that the adsorption behavior of TC on Ag(1%)-BN was favored at lower temperatures within the appropriate temperature range. ΔS and ΔH were calculated from eq 7 with ln$K$ versus $1/T$ (Figure 8b). ΔG was obtained from eq 8. All the thermodynamic parameters are presented in Table 4. The negative values of ΔH indicated an exothermic nature of adsorption, while the negative values of ΔS illustrated the decreasing randomness at the solid−liquid interface during the adsorption process. Meanwhile, the negative values of ΔG suggested that the adsorption was a spontaneous process. According to eq 8, ΔG was inversely proportional to q_e, and the smaller value of ΔG indicates a larger value of q_e. Therefore, q_e/C_e of Ag(1%)-BN/TC was larger than that of BN/TC, which also indicated that Ag(1%)-BN showed higher adsorption capacity than BN. It is well known that ΔH indicates reactive heat, which means the variation of the reactive energies. The smaller ΔH value indicated stronger interactions between TC and adsorbents.[68] Decorating AgNP onto BN changed the electronic properties of BN, making the boron atom more electropositive, resulting in the enhancement of interaction between Ag(1%)-BN and TC and the increase in adsorption capacity.

Regeneration Performance. The regeneration of an adsorbent is a key factor for its industrial application. The TC-loaded Ag(1%)-BN was eluted by 20 mL ethanol at 60 °C for regeneration. The results are shown in Figure 9. During the first two cycles, the removal efficiency had no obvious change. But after the second cycle, an obvious decline was observed. The reason maybe that after several cycles the BN stacked layer by layer caused the decrease in $\pi-\pi$ interaction. Nevertheless, the removal efficiency of Ag(1%)-BN for TC remained above 70% even after five cycles, demonstrating good regeneration performance as well as good potential in industry applications.

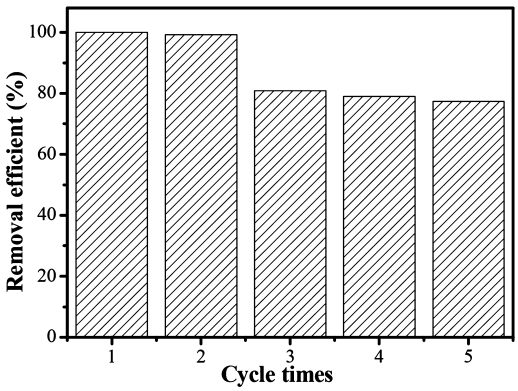

Figure 9. Recycle times of the TC removal with Ag(1%)-BN as the adsorbent.

CONCLUSIONS

In conclusion, AgNP was successfully decorated on BN by a simple one-pot pyrolysis method, and the obtained Ag-BN was proved to be a high-efficiency adsorbent. The superior adsorption performance was exhibited in terms of rapid adsorption rate, good recycling capability, and high maximum adsorption capacity (358 mg/g for TC and 880 mg/g for RhB according to the Langmuir isotherm). Importantly, the introduction of AgNP tailored the electronic properties of BN and increased its adsorption capacity. Lewis acid−base interaction, electrostatic interaction, and $\sigma-\pi$ and $\pi-\pi$ interactions played important roles in this adsorption process. We hypothesized that this novel strategy can be used to tune the electronic properties of other adsorbents for improving their adsorptive behavior.

ASSOCIATED CONTENT

Supporting Information

The Supporting Information is available free of charge on the ACS Publications Web site at the TEM images and the size distribution of Ag nanoparticles of Ag(1%)-BN, pore size and

DOI: 10.1021/acssuschemeng.7b04481
ACS Sustainable Chem. Eng. 2018, 6, 4948−4957

BET data, the RDG surface of the Ag4 cluster model and the list of adsorption capacity for other adsorbents. The Supporting Information is available free of charge on the ACS Publications website at DOI: 10.1021/acssuschemeng.7b04481.

(PDF)

AUTHOR INFORMATION

Corresponding Authors

*E-mail: chaoyh@ujs.edu.cn (Yanhong Chao).
*E-mail: zhuws@ujs.edu.cn (Wenshuai Zhu).

ORCID

Huaming Li: 0000-0002-9538-5358

Notes

The authors declare no competing financial interest.

ACKNOWLEDGMENTS

The authors are grateful for financial supported by the National Nature Science Foundation of China (21506083, 21722604, 21606113), Chinese Postdoctoral Science Foundation (2017M611726), Postdoctoral Innovation Fund of Jiangsu Province (1601254C), Key Laboratory of Tropical Medicinal Plant Chemistry of Ministry of Education, Hainan Normal University (20150376), and Scientific Research Foundation of Jiangsu University for the Senior Personnel (15JDG176).

REFERENCES

(1) Zou, Y. D.; Wang, X. X.; Ai, Y. J.; Liu, Y. H.; Li, J. X.; Ji, Y. F.; Wang, X. K. Coagulation Behavior of Graphene Oxide on Nanocrystallined Mg/AI Layered Double Hydroxides: Batch Experimental and Theoretical Calculation Study. *Environ. Sci. Technol.* **2016**, *50*, 3658−3667.

(2) Martinez Quiroz, M.; Lopez Maldonado, E. A.; Ochoa Teran, A.; Oropeza Guzman, M. T.; Pina Luis, G. E.; Zeferino Ramirez, J. Innovative Uses of Carbamoyl Benzoic Acids in Coagulation-Flocculation's Processes of Wastewater. *Chem. Eng. J.* **2017**, *307*, 981−988.

(3) Zhao, J.; Lu, Z.; He, X.; Zhang, X.; Li, Q.; Xia, T.; Zhang, W.; Lu, C. Fabrication and Characterization of Highly Porous Fe(OH)(3)@Cellulose Hybrid Fibers for Effective Removal of Congo Red from Contaminated Water. *ACS Sustainable Chem. Eng.* **2017**, *5*, 7723−7732.

(4) Wang, B.; Lv, X. L.; Feng, D. W.; Xie, L. H.; Zhang, J.; Li, M.; Xie, Y. B.; Li, J. R.; Zhou, H. C. Highly Stable Zr(IV)-Based Metal-Organic Frameworks for the Detection and Removal of Antibiotics and Organic Explosives in Water. *J. Am. Chem. Soc.* **2016**, *138*, 6204−6216.

(5) Desai, A. V.; Manna, B.; Karmakar, A.; Sahu, A.; Ghosh, S. K. A Water-Stable Cationic Metal-Organic Framework as a Dual Adsorbent of Oxoanion Pollutants. *Angew. Chem., Int. Ed.* **2016**, *55*, 7811−7815.

(6) Chao, Y. H.; Zhu, W. S.; Wu, X. Y.; Hou, F. F.; Xun, S. H.; Wu, P. W.; Ji, H. Y.; Xu, H.; Li, H. M. Application of Graphene-Like Layered Molybdenum Disulfide and Its Excellent Adsorption Behavior for Doxycycline Antibiotic. *Chem. Eng. J.* **2014**, *243*, 60−67.

(7) Huang, L.; He, M.; Chen, B.; Cheng, Q.; Hu, B. Facile Green Synthesis of Magnetic Porous Organic Polymers for Rapid Removal and Separation of Methylene Blue. *ACS Sustainable Chem. Eng.* **2017**, *5*, 4050−4055.

(8) Aramsangtienchai, P.; Spiegelman, N. A.; He, B.; Miller, S. P.; Dai, L.; Zhao, Y.; Lin, H. HDAC8 Catalyzes the Hydrolysis of Long Chain Fatty Acyl Lysine. *ACS Chem. Biol.* **2016**, *11*, 2685−2692.

(9) Hsieh, H. S.; Pignatello, J. J. Activated Carbon-Mediated Base Hydrolysis of Alkyl Bromides. *Appl. Catal., B* **2017**, *211*, 68−78.

(10) Huang, Z. F.; Song, J. J.; Pan, L.; Zhang, X. W.; Wang, L.; Zou, J. J. Tungsten Oxides for Photocatalysis, Electrochemistry, and Phototherapy. *Adv. Mater.* **2015**, *27*, 5309−5327.

(11) Li, N.; Zhang, J.; Tian, Y.; Zhao, J. H.; Zhang, J.; Zuo, W. Precisely Controlled Fabrication of Magnetic 3D Gamma-Fe_2O_3@ZnO Core-Shell Photocatalyst with Enhanced Activity: Ciprofloxacin Degradation and Mechanism Insight. *Chem. Eng. J.* **2017**, *308*, 377−385.

(12) Qiu, B.; Xing, M.; Zhang, J. Mesoporous TiO_2 Nanocrystals Grown in Situ on Graphene Aerogels for High Photocatalysis and Lithium-Ion Batteries. *J. Am. Chem. Soc.* **2014**, *136*, 5852−5855.

(13) Santoro, C.; Serov, A.; Stariha, L.; Kodali, M.; Gordon, J.; Babanova, S.; Bretschger, O.; Artyushkova, K.; Atanassov, P. Iron Based Catalysts from Novel Low-Cost Organic Precursors for Enhanced Oxygen Reduction Reaction in Neutral Media Microbial Fuel Cells. *Energy Environ. Sci.* **2016**, *9*, 2346−2353.

(14) Hu, Z.; Beuret, M.; Khan, H.; Ariya, P. A. Development of a Recyclable Remediation System for Gaseous Btex: Combination of Iron Oxides Nanoparticles Adsorbents and Electrochemistry. *ACS Sustainable Chem. Eng.* **2014**, *2*, 2739−2747.

(15) Zheng, X.; Su, J.; Wei, X.; Jiang, T.; Gao, S.; Wang, Z. L. Self-Powered Electrochemistry for the Oxidation of Organic Molecules by a Cross-Linked Triboelectric Nanogenerator. *Adv. Mater.* **2016**, *28*, 5188−5194.

(16) Ahmad, M.; Liu, S. T.; Mahmood, N.; Mahmood, A.; Ali, M.; Zheng, M. S.; Ni, J. R. Synergic Adsorption-Biodegradation by an Advanced Carrier for Enhanced Removal of High-Strength Nitrogen and Refractory Organics. *ACS Appl. Mater. Interfaces* **2017**, *9*, 13188−13200.

(17) Xiong, H. F.; Zou, D. L.; Zhou, D. D.; Dong, S. S.; Wang, J. W.; Rittmann, B. E. Enhancing Degradation and Mineralization of Tetracycline Using Intimately Coupled Photocatalysis and Biodegradation (ICPB). *Chem. Eng. J.* **2017**, *316*, 7−14.

(18) Yang, R.; Li, H. J.; Huang, M.; Yang, H.; Li, A. M. A Review on Chitosan-Based Flocculants and Their Applications in Water Treatment. *Water Res.* **2016**, *95*, 59−89.

(19) Lei, W. W.; Portehault, D.; Liu, D.; Qin, S.; Chen, Y. Porous Boron Nitride Nanosheets for Effective Water Cleaning. *Nat. Commun.* **2013**, *4*, 1777−1783.

(20) Xiong, J.; Li, H. M.; Yang, L.; Luo, J.; Chao, Y. H.; Pang, J. Y.; Zhu, W. S. Metal-Free Boron Nitride Adsorbent for Ultra-Deep Desulfurization. *AIChE J.* **2017**, *63*, 3463−3469.

(21) Wang, J. M.; Hao, J.; Liu, D.; Qin, S.; Chen, C.; Yang, C.; Liu, Y. C.; Yang, T. Y.; Fan, Y.; Chen, Y.; Lei, W. W. Flower Stamen-Like Porous Boron Carbon Nitride Nanoscrolls for Water Cleaning. *Nanoscale* **2017**, *9*, 9787−9791.

(22) Ding, J. J.; Zhu, J.; Li, Y. X.; Liu, X. Q.; Sun, L. B. Smart Adsorbents Functionalized with Thermoresponsive Polymers for Selective Adsorption and Energy-Saving Regeneration. *Ind. Eng. Chem. Res.* **2017**, *56*, 4341−4349.

(23) Patra, A. K.; Kim, D. Smart Design of Self-Assembled Mesoporous Alpha-FeOOH Nanoparticles: High-Surface-Area Sorbent for Hg^{2+} from Wastewater. *ACS Sustainable Chem. Eng.* **2017**, *5*, 1272−1279.

(24) Shen, L. J.; Cao, Y. N.; Du, Z. J.; Zhao, W. T.; Lin, K.; Jiang, L. L. Illuminate the Active Sites of Gamma-FeOOH for Low-Temperature Desulfurization. *Appl. Surf. Sci.* **2017**, *425*, 212−219.

(25) Wang, J.; Liu, J.; Zhou, Y. C.; Hodgson, P.; Li, Y. C. One-Pot Facile Synthesis of Hierarchical Hollow Microspheres Constructed with MnO_2 Nanotubes and Their Application in Lithium Storage and Water Treatment. *RSC Adv.* **2013**, *3*, 25937−25943.

(26) Liu, Y.; Luo, C.; Sun, J.; Li, H. Z.; Sun, Z. B.; Yan, S. Q. Enhanced Adsorption Removal of Methyl Orange from Aqueous Solution by Nanostructured Proton-Containing Delta-MnO_2. *J. Mater. Chem. A* **2015**, *3*, 5674−5682.

(27) Nayak, A. K.; Lee, S.; Choi, Y. I.; Yoon, H. J.; Sohn, Y.; Pradhan, D. Crystal Phase and Size-Controlled Synthesis of Tungsten Trioxide Hydrate Nanoplates at Room Temperature: Enhanced Cr(VI) Photoreduction and Methylene Blue Adsorption Properties. *ACS Sustainable Chem. Eng.* **2017**, *5*, 2741−2750.

(28) Adachi, K.; Watanabe, K.; Yamazaki, S. Ph-Responsive Switchable Aggregation Phenomena of Xanthene Dyes Adsorbed on

DOI: 10.1021/acssuschemeng.7b04481
ACS Sustainable Chem. Eng. 2018, 6, 4948−4957

Tungsten(VI) Oxide Colloid Surface. *Ind. Eng. Chem. Res.* **2014**, *53*, 13046−13057.
(29) Wee, L. H.; Meledina, M.; Turner, S.; Van Tendeloo, G.; Zhang, K.; Rodriguez-Albelo, L. M.; Masala, A.; Bordiga, S.; Jiang, J.; Navarro, J. A. R.; Kirschhock, C. E. A.; Martens, J. A. 1D-2D-3D Transformation Synthesis of Hierarchical Metal-Organic Framework Adsorbent for Multicomponent Alkane Separation. *J. Am. Chem. Soc.* **2017**, *139*, 819−828.
(30) Li, P. Z.; Wang, X. J.; Tan, S. Y.; Ang, C. Y.; Chen, H. Z.; Liu, J.; Zou, R. Q.; Zhao, Y. L. Clicked Isoreticular Metal-Organic Frameworks and Their High Performance in the Selective Capture and Separation of Large Organic Molecules. *Angew. Chem., Int. Ed.* **2015**, *54*, 12748−12752.
(31) Cheng, L.; Jiang, Y.; Yan, N.; Shan, S.-F.; Liu, X. Q.; Sun, L. B. Smart Adsorbents with Photoregulated Molecular Gates for Both Selective Adsorption and Efficient Regeneration. *ACS Appl. Mater. Interfaces* **2016**, *8*, 23404−23411.
(32) Jiang, Y.; Tan, P.; Cheng, L.; Shan, S. F.; Liu, X. Q.; Sun, L. B. Selective Adsorption and Efficient Regeneration Via Smart Adsorbents Possessing Thermo-Controlled Molecular Switches. *Phys. Chem. Chem. Phys.* **2016**, *18*, 9883−9887.
(33) Jiang, Y.; Tan, P.; Kang, Y. H.; Xing, Z. M.; Cheng, L.; Zhu, L.; Liu, X. Q.; Sun, L. B. Fabrication of Adsorbents with Thermocontrolled Molecular Gates for Both Selective Adsorption and Efficient Regeneration. *Adv. Mater. Interfaces* **2016**, *3*, 1500829−1500835.
(34) Xiong, J.; Zhu, W. S.; Li, H. P.; Yang, L.; Chao, Y. H.; Wu, P. W.; Xun, S. H.; Jiang, W.; Zhang, M.; Li, H. M. Carbon-Doped Porous Boron Nitride: Metal-Free Adsorbents for Sulfur Removal from Fuels. *J. Mater. Chem. A* **2015**, *3*, 12738−12747.
(35) Nag, A.; Raidongia, K.; Hembram, K. P. S. S.; Datta, R.; Waghmare, U. V.; Rao, C. N. R. Graphene Analogues of BN: Novel Synthesis and Properties. *ACS Nano* **2010**, *4*, 1539−1544.
(36) Pakdel, A.; Bando, Y.; Golberg, D. Nano Boron Nitride Flatland. *Chem. Soc. Rev.* **2014**, *43*, 934−959.
(37) Zhu, W. S.; Gao, X.; Li, Q.; Li, H. P.; Chao, Y. H.; Li, M. J.; Mahurin, S. M.; Li, H. M.; Zhu, H. Y.; Dai, S. Controlled Gas Exfoliation of Boron Nitride into Few-Layered Nanosheets. *Angew. Chem., Int. Ed.* **2016**, *55*, 10766−10770.
(38) Zhu, W. S.; Wu, Z. L.; Foo, G. S.; Gao, X.; Zhou, M. X.; Liu, B.; Veith, G. M.; Wu, P. W.; Browning, K. L.; Lee, H. N.; et al. Taming Interfacial Electronic Properties of Platinum Nanoparticles on Vacancy-Abundant Boron Nitride Nanosheets for Enhanced Catalysis. *Nat. Commun.* **2017**, *8*, 15291−15298.
(39) Yu, S.; Wang, X.; Pang, H.; Zhang, R.; Song, W.; Fu, D.; Hayat, T.; Wang, X. Boron Nitride-Based Materials for the Removal of Pollutants from Aqueous Solutions: A Review. *Chem. Eng. J.* **2018**, *333*, 343−360.
(40) Xue, L.; Lu, B.; Wu, Z. S.; Ge, C.; Wang, P.; Zhang, R.; Zhang, X. D. Synthesis of Mesoporous Hexagonal Boron Nitride Fibers with High Surface Area for Efficient Removal of Organic Pollutants. *Chem. Eng. J.* **2014**, *243*, 494−499.
(41) Liu, F.; Yu, J.; Ji, X. X.; Qian, M. Q. Nanosheet-Structured Boron Nitride Spheres with a Versatile Adsorption Capacity for Water Cleaning. *ACS Appl. Mater. Interfaces* **2015**, *7*, 1824−1832.
(42) Song, Q. Q.; Fang, Y.; Liu, Z. Y.; Li, L. L.; Wang, Y. R.; Liang, J. L.; Huang, Y.; Lin, J.; Hu, L.; Zhang, J.; Tang, C. The Performance of Porous Hexagonal BN in High Adsorption Capacity Towards Antibiotics Pollutants from Aqueous Solution. *Chem. Eng. J.* **2017**, *325*, 71−79.
(43) Lei, W. W.; Liu, D.; Chen, Y. Highly Crumpled Boron Nitride Nanosheets as Adsorbents: Scalable Solvent-Less Production. *Adv. Mater. Interfaces* **2015**, *2*, 1400529−1400534.
(44) Li, J.; Huang, Y.; Liu, Z. Y.; Zhang, J.; Liu, X. X.; Luo, H.; Ma, Y. H.; Xu, X. W.; Lu, Y.; Lin, J.; Zou, J.; Tang, C. C. Chemical Activation of Boron Nitride Fibers for Improved Cationic Dye Removal Performance. *J. Mater. Chem. A* **2015**, *3*, 8185−8193.
(45) Xiong, J.; Yang, L.; Chao, Y. H.; Pang, J. Y.; Zhang, M.; Zhu, W. S.; Li, H. M. Boron Nitride Mesoporous Nanowires with Doped Oxygen Atoms for the Remarkable Adsorption Desulfurization Performance from Fuels. *ACS Sustainable Chem. Eng.* **2016**, *4*, 4457−4464.
(46) Li, H. P.; Zhu, W. S.; Zhu, S. W.; Xia, J. X.; Chang, Y. H.; Jiang, W.; Zhang, M.; Zhou, Y. W.; Li, H. M. The Selectivity for Sulfur Removal from Oils: An Insight from Conceptual Density Functional Theory. *AIChE J.* **2016**, *62*, 2087−2100.
(47) Xiong, J.; Zhu, W.; Li, H.; Ding, W.; Chao, Y.; Wu, P.; Xun, S.; Zhang, M.; Li, H. Few-Layered Graphene-Like Boron Nitride Induced a Remarkable Adsorption Capacity for Dibenzothiophene in Fuels. *Green Chem.* **2015**, *17*, 1647−1656.
(48) Ma, C.; Gao, Q. Q.; Hong, W.; Fan, J.; Fang, J. X. Real-Time Probing Nanopore-in-Nanogap Plasmonic Coupling Effect on Silver Supercrystals with Surface-Enhanced Raman Spectroscopy. *Adv. Funct. Mater.* **2017**, *27*, 1603233−1603241.
(49) Dai, P. C.; Xue, Y. M.; Wang, X. B.; Weng, Q. H.; Zhang, C.; Jiang, X. F.; Tang, D. M.; Wang, X.; Kawamoto, N.; Ide, Y.; Mitome, M.; Golberg, D.; Bando, Y. Pollutant Capturing Sers Substrate: Porous Boron Nitride Microfibers with Uniform Silver Nanoparticle Decoration. *Nanoscale* **2015**, *7*, 18992−18997.
(50) Cao, H. L.; Huang, H. B.; Chen, Z.; Karadeniz, B.; Lu, J.; Cao, R. Ultrafine Silver Nanoparticles Supported on a Conjugated Microporous Polymer as High-Performance Nanocatalysts for Nitrophenol Reduction. *ACS Appl. Mater. Interfaces* **2017**, *9*, 5231−5236.
(51) Kim, C.; Jeon, H. S.; Eom, T.; Jee, M. S.; Kim, H.; Friend, C. M.; Min, B. K.; Hwang, Y. J. Achieving Selective and Efficient Electrocatalytic Activity for CO_2 Reduction Using Immobilized Silver Nanoparticles. *J. Am. Chem. Soc.* **2015**, *137*, 13844−13850.
(52) Chen, D.; Mei, X.; Ji, G.; Lu, M.; Xie, J.; Lu, J.; Lee, J. Y. Reversible Lithium-Ion Storage in Silver-Treated Nanoscale Hollow Porous Silicon Particles. *Angew. Chem.* **2012**, *124*, 2459−2463.
(53) Kim, C.; Jung, J. W.; Yoon, K. R.; Youn, D. Y.; Park, S.; Kim, I. D. A High-Capacity and Long-Cycle-Life Lithium-Ion Battery Anode Architecture: Silver Nanoparticle-Decorated SnO_2/NiO Nanotubes. *ACS Nano* **2016**, *10*, 11317−11326.
(54) Zhu, W.; Dai, B.; Wu, P.; Chao, Y.; Xiong, J.; Xun, S.; Li, H.; Li, H. Graphene-Analogue Hexagonal BN Supported with Tungsten-Based Ionic Liquid for Oxidative Desulfurization of Fuels. *ACS Sustainable Chem. Eng.* **2015**, *3*, 186−194.
(55) Zhang, Y. J.; Mori, T.; Ye, J. H.; Antonietti, M. Phosphorus-Doped Carbon Nitride Solid: Enhanced Electrical Conductivity and Photocurrent Generation. *J. Am. Chem. Soc.* **2010**, *132*, 6294−6295.
(56) She, X. J.; Wu, J. J.; Xu, H.; Mo, Z.; Lian, J. B.; Song, Y. H.; Liu, L.; Du, D. L.; Li, H. M. Enhancing Charge Density and Steering Charge Unidirectional Flow in 2D Non-Metallic Semiconductor-CNTs-Metal Coupled Photocatalyst for Solar Energy Conversion. *Appl. Catal., B* **2017**, *202*, 112−117.
(57) Marchesini, S.; Mcgilvery, C. M.; Bailey, J.; Petit, C. Template-Free Synthesis of Highly Porous Boron Nitride: Insights into Pore Network Design and Impact on Gas Sorption. *ACS Nano* **2017**, *11*, 10003−10011.
(58) Tomer, V. K.; Thangaraj, N.; Gahlot, S.; Kailasam, K. Cubic Mesoporous Ag@CN: A High Performance Humidity Sensor. *Nanoscale* **2016**, *8*, 19794−19803.
(59) Lin, Y.; Connell, J. W. Advances in 2D Boron Nitride Nanostructures: Nanosheets, Nanoribbons, Nanomeshes, and Hybrids with Graphene. *Nanoscale* **2012**, *4*, 6908−6939.
(60) Shao, W.; Liu, X. F.; Min, H. H.; Dong, G. H.; Feng, Q. Y.; Zuo, S. L. Preparation, Characterization, and Antibacterial Activity of Silver Nanoparticle-Decorated Graphene Oxide Nanocomposite. *ACS Appl. Mater. Interfaces* **2015**, *7*, 6966−6973.
(61) Di, J.; Xia, J. X.; Ji, M. X.; Wang, B.; Yin, S.; Huang, Y.; Chen, Z. G.; Li, H. M. New Insight of Ag Quantum Dots with the Improved Molecular Oxygen Activation Ability for Photocatalytic Applications. *Appl. Catal., B* **2016**, *188*, 376−387.
(62) Liu, J. J.; Zou, S. H.; Xiao, L. P.; Fan, J. Well-Dispersed Bimetallic Nanoparticles Confined in Mesoporous Metal Oxides and Their Optimized Catalytic Activity for Nitrobenzene Hydrogenation. *Catal. Sci. Technol.* **2014**, *4*, 441−446.

DOI: 10.1021/acssuschemeng.7b04481
ACS Sustainable Chem. Eng. 2018, 6, 4948−4957

(63) Lian, G.; Zhang, X.; Si, H. B.; Wang, J.; Cui, D. L.; Wang, Q. L. Boron Nitride Ultrathin Fibrous Nanonets: One-Step Synthesis and Applications for Ultrafast Adsorption for Water Treatment and Selective Filtration of Nanoparticles. *ACS Appl. Mater. Interfaces* **2013**, *5*, 12773−12778.
(64) Yang, W. B.; Zheng, F. F.; Lu, Y. P.; Xue, X. X.; Li, N. Adsorption Interaction of Tetracyclines with Porous Synthetic Resins. *Ind. Eng. Chem. Res.* **2011**, *50*, 13892−13898.
(65) Liu, Q.; Zhong, L. B.; Zhao, Q. B.; Frear, C.; Zheng, Y. M. Synthesis of Fe_3O_4/Polyacrylonitrile Composite Electrospun Nanofiber Mat for Effective Adsorption of Tetracycline. *ACS Appl. Mater. Interfaces* **2015**, *7*, 14573−14583.
(66) Zhang, L.; Song, X. Y.; Liu, X. Y.; Yang, L. J.; Pan, F.; Lv, J. N. Studies on the Removal of Tetracycline by Multi-Walled Carbon Nanotubes. *Chem. Eng. J.* **2011**, *178*, 26−33.
(67) Johnson, E. R.; Keinan, S.; Mori-Sanchez, P.; Contreras-Garcia, J.; Cohen, A.; Yang, W. Revealing Noncovalent Interactions. *J. Am. Chem. Soc.* **2010**, *132*, 6498−6506.
(68) Li, H. P.; Chang, Y. H.; Zhu, W. S.; Jiang, W.; Zhang, M.; Xia, J. X.; Yin, S.; Li, H. M. A DFT Study of the Extractive Desulfurization Mechanism by $[Bmim]^+[AlCl_4]^-$ Ionic Liquid. *J. Phys. Chem. B* **2015**, *119*, 5995−6009.
(69) Meng, A.; Xing, J.; Li, Z. J.; Li, Q. D. Cr-Doped ZnO Nanoparticles: Synthesis, Characterization, Adsorption Property, and Recyclability. *ACS Appl. Mater. Interfaces* **2015**, *7*, 27449−27457.
(70) Gao, H. C.; Sun, Y. M.; Zhou, J. J.; Xu, R.; Duan, H. W. Mussel-Inspired Synthesis of Polydopamine-Functionalized Graphene Hydrogel as Reusable Adsorbents for Water Purification. *ACS Appl. Mater. Interfaces* **2013**, *5*, 425−432.
(71) Niwas, R.; Gupta, U.; Khan, A. A.; Varshney, K. G. The Adsorption of Phosphamidon on the Surface of Styrene Supported Zirconium (IV) Tungstophosphate: A Thermodynamic Study. *Colloids Surf., A* **2000**, *164*, 115−119.

DOI: 10.1021/acssuschemeng.7b04481
ACS Sustainable Chem. Eng. 2018, 6, 4948−4957